Investigation of the Electrochemical Active Thickness of Solid Oxide Fuel Cell Anode

Keqing Zheng[1], Li Li[2], Meng Ni*,[1]

[1] Building Energy Research Group, Department of Building and Real Estate
The Hong Kong Polytechnic University, Hung Hom, Kowloon, Hong Kong

[2] Ability R&D Energy Research Centre, School of Energy and Environment
City University of Hong Kong, Hong Kong, China

Abstract

Determination of the electrochemical active thickness (EAT) is of paramount importance for optimizing the solid oxide fuel cell (SOFC) electrode. However, very different EAT values are reported in the previous literatures. This paper aims to systematically study the EAT of SOFC anode numerically. A SOFC model coupling electrochemical reactions with transport of gas, electron and ion is developed. The microstructure features of the electrode are modeled based on the percolation theory and coordinate number theory. Parametric analysis is performed to examine the effects of various operating conditions and microstructures on EAT. Results indicate that EAT increases with decreasing exchange current density (or decreasing TPB length) and increasing effective ionic conductivity. In addition to the numerical simulations, theoretical analysis is conducted including various losses in the electrode, which clearly shows that the EAT highly depends on the ratio of concentration related activation loss $R_{act,con}$ to ohmic loss R_{ohmic}. The theoretical analysis explains very well the different EATs reported in the literature and is different from the common understanding that the EAT is controlled mainly by the ionic conductivity of electrode.

Keywords: Solid oxide fuel cell; Model; Anode; Electrochemical active thickness

* Corresponding author. Tel: (852) 2766 4152; Fax: (852) 2764 5131;
Email: bsmengni@polyu.edu.hk (Meng Ni)

Nomenclature

j	electric current density, A/m^2
j_{TPB}	electric current generated in unit TPB length, A/m
j_{ref}	reference exchange current density, A/m
p	partical pressure, pa
p_{atm}	operating pressure, pa
r	particle radius, m
r_p	pore radius, m
n_{el}	particle number of electron conducting particles
x	gas molar fraction
$B_{A/C}$	anode/channel interface
$B_{C/C}$	cathode/channel interface
$B_{A/E}$	anode/electrolyte interface
$B_{C/E}$	cathode/electrolyte interface
$D_{i,k}^{eff}$	effective Knudsen diffusion coefficient of gas species i, m^2/s
$D_{i,l}^{eff}$	effective binary diffusion coefficient of gas species i and l, m^2/s
E_{eq}	equilibrium electric potential difference, V
E_{Nernst}	reversible electrode potential, V
F	Faraday constant, 96485 C/mol
$L_{el\text{-}io}$	perimeter of contact area between electron and ionic particles, m
L^a	anode thickness
M	molecular mass, kg/mol
N	molar flux of gas species, mol/(m^2 s)

P_{erco}	percolation possibility
R_{ohmic}	ohmic loss, V
R_{act}	activation loss, V
R_{con}	concentration loss, V
$R_{act,con}$	concentration related activation loss, V
R	ideal gas constant, 8.314 J/(mol K)
T	operating temperature, K
$Z_{el\text{-}io}$	average ionic particle number around electron particle
V_{cell}	output voltage, V

Greek letters

η_{local}	overpotential, V
ϕ	electric potential, V
σ	effective conductivity, S/m
σ^0	material intrinsic conductivity, S/m
λ_{TPB}	TPB length in unit volume (m/m^3)
ξ	tortuosity factor for gas diffusion
v	diffusion volume (m^3/mol)
Ψ	volume fraction

Subscripts:

el	electronic conducting phase
io	ionic conducting phase
inlet	inlet conditions
ref	reference conditions
local	local reaction sites
H2	hydrogen

O2	oxygen
H2O	water
y	position *y*

Superscripts:

a	anode side
c	cathode side

1. Introduction

Solid oxide fuel cell (SOFC) has recent increasing attention in recent years for its potential in clean and efficient power generation. SOFC electrode functions as a provider of the electrochemical reaction sites as well as the transport medium of ion, electron and gas. In operation, electrochemical reactions only occur in the triple phase boundaries (TPBs, as shown in Fig. 1) where reaction gas, ion-conducting phase and electron-conducting phase meet. However, even the TPBs in SOFC electrode are percolated [1], the electrochemical reactions are believed to occur in a small depth from the electrolyte/electrode (E/E) interface, which is known as the electrochemical active thickness (EAT). Determination of the EAT is important in designing an SOFC electrode with optimum thickness [2]. If the electrode thickness is thinner than EAT, the active TPBs are reduced. If the electrode thickness is much larger than EAT, the concentration loss caused by gas transportation will also degrade SOFC performance. In addition, the accurate determination of the EAT is the prerequisite for optimizing the functionally graded electrode, in which the microstructure and material composition are purposely varied in different layers according to their functions: for electrochemical reactions, gas transport, electron conduction or ion conduction.

However, the EAT reported in literatures significantly varies probably due to the different operating conditions, electrode microstructures and material properties used

in their studies. Martin Andersson et al. [3] developed a CFD model including fully coupled heat, mass, momentum and charge transport and revealed that the reaction zone that contains 90% of the electrochemical reactions should be 2.4 μm in cathode and 6.2 μm in anode under operating temperature of 1010K. For comparison, it is reported by M. M. Hussain et al. [4] that the EAT in anode is about 20 μm when the operating temperature is 1073K, current density is 0.5 A/m^2 and average particle radius is 0.1 μm. Furthermore, it is revealed in their study that the EAT is increased to about 60 μm when operating temperature is increased to 1273 K. Yoshinori Suzue et al. [5] and Naoki Shikazono et al. [6] solved the governing equations describing gas, ion and electron transport using Lattice Boltzmann Method (LBM) based on their reconstructed Ni/YSZ anode. The positive correlation between EAT (5 μm-20 μm) and operating temperature (873 K-1073 K) is also found in their study. However, the efficient thickness examined by Z.Y. Jiang et al [7] increases from 36 μm to 126 μm with operating temperature decreases from 1073 K to 923 K, which is contradict to previous studies. It is commonly regarded that the narrow reaction zone is limited by the poor ionic conductivity of electrode, and thus high temperature should generate a large EAT due to the raised high ionic conductivity. The different operating temperature effect on EAT reported by Z.Y. Jiang et al [7] implies a more complicated underlying relationship between operating parameters and EAT. Besides, it is reported by Naoki Shikazono et al. [6] that a thinner EAT is found with 10% humidified H2 as fuel, compared with the EAT of about 10-15 μm when 1.2% humidified H2 is used as fuel at 1273K. This result also can't be explained by our common knowledge that the EAT is controlled by the electrode ionic conductivity.

This study aims to systematically investigate the EAT in SOFC anode over a wide range of operating and structural parameters. First, a numerical SOFC model is

developed, in which the concentration related Butler-Volmer (BV) equation, the ohm's law and dusty gas model (DGM) are used to describe the electrochemical kinetics in TPBs, the electron and ion transport in electrodes and electrolyte, and the gas diffusion in electrode pores. The effective conductivities and TPB length required in model calculation are obtained with models based on the percolation theory and coordinate number theory [8-9]. After that, parametric analysis is conducted to examine the effects of operating conditions and electrode microstructure parameters on EAT. Finally, explanation of results is given by a theoretical analysis of various losses in electrode.

2. Model Development

A one dimensional (1D) anode-supported planar type SOFC model is developed. The computational domain and boundaries are shown in Fig. 2. Main assumptions in this model include: (1) Constant operating temperature condition is adopted. (2) Reaction sites (TPBs) are assumed to be uniformed distributed and well percolated inside electrodes. (3) Since the convection flow and pressure gradient effect could be safely neglected [10-12], only diffusion is considered for gas transport inside the porous electrodes.

2.1 Electrochemistry

In this model, only O_2 reduction reaction and H_2 oxidation reaction are considered, as shown in Fig. 1.

Anode:

$$H_2 + O^{2-} \rightarrow H_2O + 2e^- \quad (1)$$

Cathode:

$$0.5O_2 + 2e^- \rightarrow O^{2-} \quad (2)$$

The generated oxygen ions O^{2-} in cathode are transported through electrolyte into anode while the released electrons e^- in anode are transported through external circuit to cathode to form a cycle. Therefore, the overall reaction in the cell is:

$$H_2 + 0.5O_2 \rightarrow H_2O \tag{3}$$

2.1.1 Electrochemical reaction kinetics

The relationship between electric current generated in unit TPB length j_{TPB} (A/m) and local overpotential η_{local} can be described by the Butler-Volmer equation [13-14]:

$$j^a_{TPB} = j^a_{ref}\left(\frac{p_{H2,TPB}}{p_{H2,ref}}\right)\left(\frac{p_{H2O,TPB}}{p_{H2O,ref}}\right)\left\{\exp\left(\frac{F\eta^a_{local}}{RT}\right) - \exp\left(\frac{-F\eta^a_{local}}{RT}\right)\right\} \tag{4}$$

$$j^c_{TPB} = j^c_{ref}\left(\frac{p_{O2,TPB}}{p_{O2,ref}}\right)^{0.25}\left\{\exp\left(\frac{F\eta^c_{local}}{RT}\right) - \exp\left(\frac{-F\eta^c_{local}}{RT}\right)\right\} \tag{5}$$

where, $p_{H2,TPB}$ and $p_{H2O,TPB}$ are the partial pressures of hydrogen and water in anode TPBs; $p_{O2,TPB}$ is the partial pressure of oxygen in cathode TPBs; $p_{H2,ref}$, $p_{H2O,ref}$ and $p_{O2,ref}$ are the reference partial pressures of hydrogen, water and oxygen (equals to 0.968 atm,0.032 atm and 0.21atm in this study, respectively); F, R, and T are the Faraday constant (96485 C/mol), ideal gas constant (8.314 J/(mol K)) and operating temperature (K); superscripts a and c represent the anode and cathode, respectively. j_{ref} is the exchange current density tested under reference conditions and it can be calculated as [13-14]:

$$j^a_{ref} = 2\times10^{-3}\times\exp\left(\frac{-85[kJ/mol]}{R}\left(\frac{1}{T} - \frac{1}{1073[K]}\right)\right) \tag{6}$$

$$j^c_{ref} = 3.75\times10^{-4}\times\exp\left(\frac{-100[kJ/mol]}{R}\left(\frac{1}{T} - \frac{1}{1073[K]}\right)\right) \tag{7}$$

2.1.2 Output voltage

The local overpotentials η^a_{local} and η^c_{local} in anode and cathode, and the cell output voltage V_{cell} are defined as [15]:

$$\eta^c_{local} = \phi^c_{el} - \phi^c_{io} - E^c_{eq} \tag{8}$$

$$\eta^a_{local} = \phi^a_{el} - \phi^a_{io} - E^a_{eq} \tag{9}$$

$$V_{cell} = \phi^{C/C}_{el} - \phi^{A/C}_{el} \tag{10}$$

where, ϕ and E_{eq} are the electric potential (V) and equilibrium electric potential difference (V), respectively; subscripts *el* and *io* represent the electronic phase and ionic phase; superscripts *a* and *c* represent the anode and cathode, respectively; superscripts *C/C* and *A/C* represent boundaries labeled in Fig. 2.

In this study, the equilibrium electric potential differences of the anode and cathode are defined as follows:

$$E^a_{eq} = 0; \quad E^c_{eq} = E_{Nernst} \tag{11}$$

where, E_{Nernst} is the reversible electrode potential and can be obtained as [16]:

$$E_{Nernst} = E_T - \frac{RT}{2F}\ln\left(\frac{p_{H2O,TPB}}{p_{H2,TPB}\,p^{0.5}_{O2,TPB}}\right) \tag{12}$$

$$E_T = 1.253 - 0.00024516T \tag{13}$$

The electric potential distribution can be obtained by solving charge balance equations [15], as written in Eq. (14)-Eq. (16).

Anode:

$$\frac{dj^a_{el}}{dy} = -\frac{dj^a_{io}}{dy} = -\sigma^a_{el}\frac{d^2\phi^a_{el}}{dy^2} = -j^a_{TPB}\lambda^a_{TPB} \tag{14}$$

Cathode:

$$\frac{dj^c_{el}}{dy} = -\frac{dj^c_{io}}{dy} = -\sigma^c_{el}\frac{d^2\phi^c_{el}}{dy^2} = j^c_{TPB}\lambda^c_{TPB} \tag{15}$$

Electrolyte:

$$\frac{dj_{io}}{dy} = -\sigma_{io}\frac{d^2\phi_{io}}{dy^2} = 0 \tag{16}$$

where, j, σ and λ_{TPB} are the electric current (A/m^2), effective conductivity (S/m) and TPB length in unit volume (m/m^3).

The percolation theory based model [8-9] is used to calculate the effective ionic conductivity σ_{io}, electronic conductivity σ_{el} and TPB length λ_{TPB}, as follows (more details can be found in ref. [8-9]):

TPB length:

$$\lambda_{TPB}^{i} = L_{el-io}^{i} n_{el}^{i} Z_{el-io}^{i} P_{erco,el}^{i} P_{erco,io}^{i} \quad i = a, c \tag{17}$$

where, $L_{el\text{-}io}$ is the perimeter of contact area between *el* and *io* particles; n_{el} is the total particle number of *el* particles; $Z_{el\text{-}io}$ is the average *io* particle number around *el* particle; P_{erco} is the percolation possibility.

Conductivity:

$$\sigma_i = \sigma_i^0 \left[(1-\varepsilon)\psi_i P_{erco,i} \right]^{1.5} \quad i = el\ ,\ io \tag{18}$$

where, ε is the electrode porosity; Ψ is the volume fraction; σ^0 is material intrinsic conductivity. In this work, materials used in anode/electrolyte/cathode are NiO+YSZ/YSZ/LSM+YSZ. However, the model can be easily applied to other materials if their material properties are known.

2.2 Mass conservation

For SOFC in operation, reactant gases (H_2 and O_2) should be transported from gas channels to TPBs while produced water steam from TPBs to gas channels. The gas concentration distributions could affect electrochemical reaction rates and further SOFC performance, as shown in Eq. (4)-Eq. (5). Gas diffusion in porous electrodes can be described by the dusty gas model (DGM) [17]:

$$\frac{N_i}{D_{i,k}^{eff}} + \sum_{l=1,l\neq i}^{n} \frac{p_l N_i - p_i N_l}{p_{atm} D_{i,l}^{eff}} = -\frac{1}{RT}\frac{dp_i}{dy} \tag{19}$$

where, N is the molar flux of gas species (mol/(m^2 s)); p and p_{atm} are the partial pressure of gas species and operating pressure (Pa); $D_{i,k}^{eff}$ is the effective Knudsen diffusion coefficient of gas species i (m^2/s); $D_{i,l}^{eff}$ is the effective binary diffusion coefficient of gas species i and l (m^2/s).

The effective diffusion coefficients can be calculated as follows [18]:

$$D_{i,k}^{eff} = \frac{\varepsilon}{\xi}\frac{2}{3} r_p \sqrt{\frac{8RT}{\pi M_i}} \tag{20}$$

$$D_{i,l}^{eff} = \frac{\varepsilon}{\xi}\frac{3.198\times10^{-8} T^{1.75}}{p_{atm}\left[v_i^{1/3} + v_l^{1/3}\right]^2}\left(\frac{1}{M_i} + \frac{1}{M_l}\right)^{0.5} \tag{21}$$

where, M is the molecular mass (kg/mol); r_p is the average pore radius (m); ξ is the tortuosity factor for gas diffusion; v is the diffusion volume (for H_2, O_2, N_2, H_2O, the values are (m^3/mol): 6.12×10^{-6}, 16.3×10^{-6}, 18.5×10^{-6}, 13.1×10^{-6}).

In steady state, the diffusion of gas species should satisfy mass balance, as written in Eq. (22) and Eq. (23).

Anode:

$$\frac{dN_{H2}}{dy} = -\frac{dN_{H2O}}{dy} = -\frac{j_{TPB}^a \lambda_{TPB}^a}{2F} \tag{22}$$

Cathode:

$$\frac{dN_{O2}}{dy} = -\frac{j_{TPB}^c \lambda_{TPB}^c}{4F} \tag{23}$$

2.3 Boundary conditions

The detailed setting information of boundary conditions labeled in Fig. 2 is listed in Table. 1. Inlet gas compositions ($p_{H2,inlet}$, $p_{H2O,inet}$, and $p_{O2,inlet}$) are given in the

anode/channel ($B_{A/C}$) and cathode/channel ($B_{C/C}$) interfaces. Mass fluxes in $B_{A/C}$ and $B_{C/C}$ are determined by total current density j. Only ionic current flux passes through the electrolyte ($B_{A/E}$ and $B_{C/E}$). Only electronic current flux passes through the electrode/channel interfaces ($B_{A/C}$ and $B_{C/C}$).

3. Solution Method and Model Validation

The established model is implemented with the commercial finite element software COMSOL MULTIPHSICS®. Equations for ion, electron and gas transport are solved simultaneously with the default stationary nonlinear solver. With given output voltages, the gas concentration，current density and local overpotential distribution can be obtained. Grid in computational domain is refined to ensure the grid independence.

Key parameters calculated with above equations are compared with literature data (under T=1073 K) and shown in Table. 2. Cell performance is also calculated and compared with experimental results [19] for model validation, as shown in Fig. 3. In the above comparison, the structural parameters of the SOFC and the operating conditions of the experimental study are used as input parameters in the simulation: the thicknesses of anode/electrolyte/cathode are 1000/8/20 μm, the volume fraction of ionic conducting phase in anode Ψ_{io} is 0.33, and porosities of anode and cathode are 0.48 and 0.26. Other parameters used in model validation can be found in Table 3.

4. Results

To be general, the subsequent parametric simulations will focus on a standard cell with typical cell configurations. The structural parameters of the standard cell are listed in Table 3. Parametric analysis of the EAT is conducted by varying only one parameter each time. The ionic current density distribution in SOFC is shown in Fig. 4 (standard cell, output voltage V_{cell}=0.7 V). As labeled in Fig. 4, the zone thickness

inside which 99% ionic current is transferred into electronic current is defined as the EAT. In the following part of this section, only the effect of various parameters on EAT is presented. Explanation of results is given in the next section.

4.1 Effect of operating conditions

Variation of EAT with different output voltage V_{cell} is shown in Fig. 5. It can be seen that the EAT increases from 5.75 μm to 9.5 μm as the output voltage V_{cell} increases from 0.3 V to 0.9 V. For comparison, it is also predicted by [2, 14] that high electrode overpotential leads to a smaller active thickness. However, [4] considered that the output voltage V_{cell} only had negligible effect on EAT. It should be noted that in the following part, results are only obtained under output voltage V_{cell}=0.8 V and V_{cell}=0.5 V for actual operation consideration.

In this study, humidified H_2 is supplied as fuel. Four kinds of $x_{H2,inlet}$ are considered to simulate the different gas composition along gas flow channel for SOFC in operation. As shown in Fig. 6, the EAT decreases from 8.1 μm to 4.5 μm as $x_{H2,inlet}$ decreases from 96.8% to 70% when output voltage V_{cell}= 0.8V. Similar results can be found in [6], in which a thinner EAT is obtained with a lower $x_{H2,inlet}$.

The effect of operating temperature T on EAT is examined by changing T from 1173 K to 873 K, as shown in Fig. 7. It can be found that the EAT increases from 8.1 μm to 9.4 μm under V_{cell}=0.8V as operating temperature T decreases from 1173K to 873K, which is consistent with results in [7]. On the contrary, [5, 14, 4, 26] revealed that the EAT was negatively correlated with operating temperature T.

Reference exchange current density is an indicator of the electrochemical reaction rate in electrode, which strongly depends on the operating conditions, electrochemical reaction types as well as electrode material properties. Since the expressions of reference exchange current density reported in literature vary significantly, it is

necessary to consider the effect of j_{ref} on EAT. The reference exchange current density j_{ref} calculated with Eq. (6) is defined as $j_{ref\_standard}$. The effect of j_{ref} on EAT is examined by changing j_{ref} from $0.1j_{ref\_standard}$ to $2j_{ref\_standard}$, as shown in Fig. 8. It can be seen that increasing exchange current density decreases the EAT, which coincides with results in [14]. Since the TPB length λ_{TPB} affects the local current source (see Eq. (14) and Eq. (4)) and further the cell performance in the same way as reference exchange current density j_{ref}, a negative correlation between λ_{TPB} and EAT can be deduced.

Similarly, effective ionic conductivity σ_{io} in anode calculated with Eq. (18) is defined as the $\sigma_{io\_standard}$. The effect of σ_{io} on EAT is examined by changing σ_{io} from $0.5\sigma_{io\_standard}$ to $2\sigma_{io\_standard}$. As shown in Fig. 9, the anode EAT increases significantly (from 5.5 μm to 15.25 μm, under V_{cell}=0.8 V) with increasing anode effective ionic conductivity. Same results can be found in [7].

4.2 Effect of structure parameters

Variations of microstructure parameters will affect electrode TPB density, effective conductivities, and effective diffusion coefficients. The effect of mean particle radius r on EAT is studied by changing the mean particle radius r from 0.5 μm to 2 μm, as shown in Fig. 10. It can be seen that EAT increases greatly from 3.75 μm to 18 μm (under V_{cell}=0.8 V) as r increases. In this aspect, similar trends are obtained in [7, 14, 27].

The effect of particle radius ratio r_{io}/r_{el} on EAT is also examined, as shown in Fig. 11. When the volume fraction of ionic conducting phase Ψ_{io} and electron particle radius r_{el} in anode are kept as 0.5 and 0.5μm, the EAT has an increase from 6.1 μm to 8.75 μm (under V_{cell}=0.8 V) as r_{io} in anode increases from 0.5 μm to 1 μm. But it is

noted by [14] that the effect of r_{io}/r_{el} on EAT depends on the resulted variation of σ_{io} and λ_{TPB}.

Variation of electrode composition changes the effective conductivities and TPB density simultaneously. Fig. 12 shows the effect of the volume fraction of electron conducting phase Ψ_{el} on EAT. Same with [7, 14, 4], a larger EAT is obtained with a lower content of the electron conducting phase Ψ_{el}.

Finally, the effect of porosity ε on EAT is examined by changing ε from 0.3 to 0.6. Increasing of porosity will decrease TPB density and effective ionic/electronic conductivity, but improve the gas transport in electrode simultaneously. Negligible effect of porosity on EAT is found in this study, as shown in Fig. 13. However, a large EAT is found with a large porosity in [14].

5. **Discussion**

To explain the results given above, various kinds of losses in SOFC anode are shown in Fig. 14. The total electrode thickness is L^a, and the original point refers to the anode/channel ($B_{A/C}$) interface. Therefore, the losses for position y to generate a certain amount of electronic current j_y (or consume a certain amount of ionic current) include: the ohmic loss caused by ion transport from $B_{A/E}$ to position y and electron transport from position y to $B_{A/C}$ (R_{ohmic}), the activation loss caused by the electrochemical process (R_{act}), and the concentration loss caused by the concentration differences between position y and reference conditions (R_{con}). Since the gas concentration distribution affects the SOFC performance by affecting the reaction rate, the R_{con} and R_{act} can be combined into $R_{act,con}$, as shown in Eq. (4). Therefore, the total voltage loss for position y to generate j_y is ($R_{act,con}$+ R_{ohmic}), which determines the possibility of the electrochemical reactions' occurrence in position y. That is, for optional position *y1* and *y2*, to generate the same amount of electronic current, if the

($R_{act,con,y1}$+$R_{ohmic,y1}$) is less than ($R_{act,con,y2}$+$R_{ohmic,y2}$), electrochemical reactions prefer to occur in position *y1*.

Based on the analysis above, two extreme situations are considered:

(1) $R_{act,con}$ is negligible and R_{ohmic} is the dominant loss. Considering the electronic conductivity is orders of magnitude larger than ionic conductivity in typical SOFC composite electrodes, its contribution to R_{ohmic} can be neglected. Therefore, R_{ohmic} is reversely proportional to the ionic transport distance. That is, the nearer the location from the anode/electrolyte interface ($B_{A/E}$), the easier for the electrochemical reactions' occurrence.

(2) R_{ohmic} is negligible and $R_{act,con}$ is the dominant loss. The gas concentration distribution effect can be ignored in typical SOFC operating conditions. As a result, the activation loss related to electrochemical reactions should be independent of its location. That is, electrochemical reactions should occur evenly throughout the electrode when homogeneous distribution of TPB is assumed.

Therefore, it can be concluded that the EAT (thickness of the reaction zone where most electrochemical reactions occur) depends on the ratio of $R_{act,con}/R_{ohmic}$ in SOFC electrode. A larger ratio will lead to a more even distribution of electrochemical reactions inside electrode and thus a larger EAT. For comparison, a lower ratio will limit the electrochemical reactions close to the electrolyte and lead to non-uniform distribution of the reaction rates.

Explanation of results:

First of all, large exchange current density j_{ref} (Fig. 8) and TPB length λ_{TPB} lead to thinner EATs by decreasing the $R_{act,con}$. Large ionic conductivity σ_{io} (Fig. 9) lead to a larger EAT by decreasing the R_{ohmic}.

As the output voltage V_{cell} decreases from 0.9 to 0.3, the dominant loss that

determines SOFC actual performance changes from the activation loss to ohmic loss, which leads to a smaller ratio of $R_{act,con}/R_{ohmic}$ and a thinner EAT, as shown in Fig. 5. But it should be noted that, different conclusions might exist when concentration loss is dominant. Moreover, the typical output voltages (0.8 V and 0.5 V) shown in the result section represent the activation loss dominant case and ohmic dominant case, respectively.

High inlet hydrogen molar fraction $x_{H2,inlet}$ causes a low reaction rate in anode (see Eq. (4)) and thus leads to a larger ratio of $R_{act,con}/R_{ohmic}$ and a thicker EAT, as shown in Fig. 6. However, it should be mentioned that high inlet oxygen molar fraction $x_{O2,inlet}$ improves the electrochemical reaction in the cathode side and indicates a thinner EAT.

Decreasing the operating temperature T decreases the reaction rate and effective conductivity simultaneously. Therefore, the effect of operating temperature on EAT depends on the resulted variation in $R_{act,con}/R_{ohmic}$. Moreover, variations in mean particle radius r, particle radius ratio r_{io}/r_{el}, porosity and volume fraction of electron conducting phase Ψ_{el} also affect the $R_{act,con}$ and R_{ohmic} at the same time. However, under wider operating conditions, the concentration could become significant or even limiting. Thus the effects of these structural parameters on electrode active thickness could be significant. Consequently, their effects on EAT require further study for a detailed cell.

6. Conclusion

In this work, a numerical model is established to investigate the EAT in SOFC anode. For the standard cell defined with parameters in Table. 3, the EAT is 8.1 μm (V_{cell}=0.8 V). Such a small value is in the range of [5, 6, 26, 28, 29], but differs a lot from [7, 25, 30]. The differences are probably caused by the quite different exchange

current densities used in simulations. The effects of various operating conditions and electrode microstructure parameters on EAT can be explained by the variation of the ratio $R_{act,con}/R_{ohmic}$. It can be concluded that measures which raise the ratio will lead to a larger EAT. Although this work is conducted for SOFC anode, the positive correlation between EAT and the ratio $R_{act,con}/R_{ohmic}$ is also applicable for SOFC cathode.

Acknowledgement

This research was supported by a grant (Project Number: PolyU5326/12E) from Research Grant Council, University Grants Committee, Hong Kong SAR.

References

[1] P. Costamagna, P. Costa, V. Antonucci, Micro-modelling of solid oxide fuel cell electrodes, Electrochim. Acta. 43 (1998) 375-394.

[2] Q. Cai, C.S. Adjiman, N.P. Brandon, Investigation of the active thickness of solid oxide fuel cell electrodes using a 3D microstructure model, Electrochim. Acta. 56 (2011) 10809-10819.

[3] M. Andersson, J. Yuan, B. Sundén, SOFC modeling considering electrochemical reactions at the active three phase boundaries, Int. J. Heat Mass Transfer. 55 (2012) 773-788.

[4] M. Hussain, X. Li, I. Dincer, A numerical investigation of modeling an SOFC electrode as two finite layers, Int J Hydrogen Energy. 34 (2009) 3134-3144.

[5] Y. Suzue, N. Shikazono, N. Kasagi, Micro modeling of solid oxide fuel cell anode based on stochastic reconstruction, J. Power Sources. 184 (2008) 52-59.

[6] N. hikazono, D. Kanno, K. Matsuzaki, H. Teshima, S. Sumino, N. Kasagi, Numerical assessment of SOFC anode polarization based on three-dimensional model microstructure reconstructed from FIB-SEM images, J. Electrochem. Soc. 157 (2010) B665-B672.

[7] Z. Jiang, C. Xia, F. Chen, Efficient thickness of solid oxide fuel cell composite electrode, Chinese Journal of Chemical Physics. 23 (2010) 217.

[8] D. Chen, L. Lu, J. Li, Z. Yu, W. Kong, H. Zhu, Percolation micro-model to predict the effective properties of the composite electrode with poly-dispersed particle sizes, J. Power Sources. 196 (2011) 3178-3185.

[9] D. Chen, Z. Lin, H. Zhu, R.J. Kee, Percolation theory to predict effective properties of solid oxide fuel-cell composite electrodes, J. Power Sources. 191 (2009) 240-252.

[10] M. Ni, D.Y.C. Leung, M.K.H. Leung, Importance of pressure gradient in solid oxide fuel cell electrodes for modeling study, J. Power Sources. 183 (2008) 668-673.

[11] Y. Vural, L. Ma, D.B. Ingham, M. Pourkashanian, Comparison of the multicomponent mass transfer models for the prediction of the concentration overpotential for solid oxide fuel cell anodes, J. Power Sources. 195 (2010) 4893-4904.

[12] M. García-Camprubí, A. Sánchez-Insa, N. Fueyo, Multimodal mass transfer in solid-oxide fuel-cells, Chemical Engineering Science. 65 (2010) 1668-1677.

[13] J.H. Nam, D.H. Jeon, A comprehensive micro-scale model for transport and reaction in intermediate temperature solid oxide fuel cells, Electrochim. Acta. 51 (2006) 3446-3460.

[14] D. Chen, W. Bi, W. Kong, Z. Lin, Combined micro-scale and macro-scale modeling of the composite electrode of a solid oxide fuel cell, J. Power Sources. 195 (2010) 6598-6610.

[15] T.X. Ho, P. Kosinski, A.C. Hoffmann, A. Vik, Modeling of transport, chemical and electrochemical phenomena in a cathode-supported SOFC, Chemical Engineering Science. 64 (2009) 3000-3009.

[16] M. Ni, M.K.H. Leung, D.Y.C. Leung, Parametric study of solid oxide fuel cell performance, Energy Conversion and Management. 48 (2007) 1525-1535.

[17] R. Suwanwarangkul, E. Croiset, M.W. Fowler, P.L. Douglas, E. Entchev, M.A. Douglas, Performance comparison of Fick's, dusty-gas and Stefan–Maxwell models to predict the concentration overpotential of a SOFC anode, J. Power Sources. 122 (2003) 9-18.

[18] W. Kong, H. Zhu, Z. Fei, Z. Lin, A modified dusty gas model in the form of a Fick's model for the prediction of multicomponent mass transport in a solid oxide fuel cell anode, J. Power Sources. 206 (2012) 171-178.

[19] F. Zhao, A.V. Virkar, Dependence of polarization in anode-supported solid oxide fuel cells on various cell parameters, J. Power Sources. 141 (2005) 79-95.

[20] A.M. Gokhale, S. Zhang, M. Liu, A stochastic geometry based model for total triple phase boundary length in composite cathodes for solid oxide fuel cells, J. Power Sources. 194 (2009) 303-312.

[21] J.R. Ferguson, J.M. Fiard, R. Herbin, Three-dimensional numerical simulation for various geometries of solid oxide fuel cells, J. Power Sources. 58 (1996) 109-122.

[22] U. Anselmi-Tamburini, G. Chiodelli, M. Arimondi, F. Maglia, G. Spinolo, Z.A. Munir, Electrical properties of Ni/YSZ cermets obtained through combustion synthesis, Solid State Ionics. 110 (1998) 35-43.

[23] W. Kiatkittipong, T. Tagawa, S. Goto, S. Assabumrungrat, P. Praserthdam, Oxygen transport through LSM/YSZ/LaAlO system for use of fuel cell type reactor, Chem. Eng. J. 106 (2005) 35-42.

[24] B. Todd, J.B. Young, Thermodynamic and transport properties of gases for use in solid oxide fuel cell modelling, J. Power Sources. 110 (2002) 186-200.

[25] S. Chan, Z. Xia, Anode micro model of solid oxide fuel cell, J. Electrochem. Soc. 148 (2001) A388-A394.

[26] S. Primdahl, M. Mogensen, Oxidation of Hydrogen on Ni/Yttria□Stabilized Zirconia Cermet Anodes, J. Electrochem. Soc. 144 (1997) 3409-3419.

[27] S. Chan, X. Chen, K. Khor, Cathode micromodel of solid oxide fuel cell, J. Electrochem. Soc. 151 (2004) A164-A172.

[28] Z. Wang, N. Zhang, J. Qiao, K. Sun, P. Xu, Improved SOFC performance with continuously graded anode functional layer, Electrochemistry Communications. 11 (2009) 1120-1123.

[29] M. Brown, S. Primdahl, M. Mogensen, Structure/Performance Relations for Ni/Yttria-Stabilized Zirconia Anodes for Solid Oxide Fuel Cells, J. Electrochem. Soc. 147 (2000) 475-485.
[30] Z. Xia, S. Chan, K. Khor, An improved anode micro model of SOFC, Electrochemical and solid-state letters. 7 (2004) A63-A65.

List of Tables

List of Figures

Table.1

	$B_{A/C}$	$B_{A/E}$	$B_{C/E}$	$B_{C/C}$
Ionic charge balance	$\overrightarrow{j_{io}^{a}} \cdot \vec{n} = 0$	$\overrightarrow{j_{io}^{a}} \cdot \vec{n} = j$	$\overrightarrow{j_{io}^{c}} \cdot \vec{n} = j$	$\overrightarrow{j_{io}^{c}} \cdot \vec{n} = 0$
Electronic charge balance	0	$\overrightarrow{j_{el}^{a}} \cdot \vec{n} = 0$	$\overrightarrow{j_{el}^{c}} \cdot \vec{n} = 0$	V_{cell}
Mass balance	$p_{\text{H2,inlet}}$ $p_{\text{H2O,inlet}}$	$\overrightarrow{N_{H2}} \cdot \vec{n} = 0$ $\overrightarrow{-N_{H2O}} \cdot \vec{n} = 0$	$\overrightarrow{N_{O2}} \cdot \vec{n} = 0$ $\overrightarrow{N_{N2}} \cdot \vec{n} = 0$	$p_{\text{O2,inlet}}$

Table. 2

Parameters	Present study	Previous study	Calculation conditions
j_{TPB}^{a}	1.62×10^{-2} A/m	1.89×10^{-2} A/m [13]	$p_{H2}=0.9\times10^{5}$ Pa $p_{H2O}=0.1\times10^{5}$ Pa $p_{O2}=0.15\times10^{5}$ Pa η_{local}^{a} =0.1 V η_{local}^{c} =0.3 V
j_{TPB}^{c}	8.83×10^{-3} A/m	1.12×10^{-2} A/m [13]	
λ_{TPB}^{a} & λ_{TPB}^{c}	1.2×10^{12} m/m^3	2.13×10^{12} m/m^3 [20]	ε=0.4 ξ=3 Ψ_{io}=0.5 $r_{io}=r_{el}=r_{p}=0.5$ μm $\sigma_{YSZ}^{0}=3.34\times10^{4}\exp(-\frac{10300}{T})$ [21] $\sigma_{Ni}^{0}=3.27\times10^{6}-1065.3\,T$ [22] $\sigma_{LSM}^{0}=\frac{8.85\times10^{7}}{T}\exp(\frac{1082.5}{T})$ [23]
σ_{io}^{a} & σ_{io}^{c}	0.33 S/m		
σ_{el}^{a}	3.1×10^{5} S/m		
σ_{el}^{c}	3.3×10^{4} S/m		
$D_{H2,k}^{eff}$	1.6×10^{-4} m^2/s	1.5×10^{-4} m^2/s [13]	
$D_{H2,H2O}^{eff}$	8.5×10^{-4} m^2/s	$5\sim9\times10^{-4}$ m^2/s [24]	

Table. 3

Operating temperature, T	1073K
Operating pressure, p	101325 Pa
Inlet gas composition (molar fraction):	
Anode, $x_{H2} + x_{H2O}$	96.8% H_2+3.2% H_2O [25]
Cathode, $x_{O2} + x_{N2}$	21% O_2+79% N_2
Structure parameter:	
Thickness, $L^a/L^e/L^c$	400 μm /50 μm /50 μm
Porosity, ε^a & ε^c	0.4
Tortuosity, ξ^a & ξ^c	3
Mean particle radius, r_{el} & r_{io}	0.5 μm
Volume fraction of ionic phase, ψ_{io}^a & ψ_{io}^c	0.5

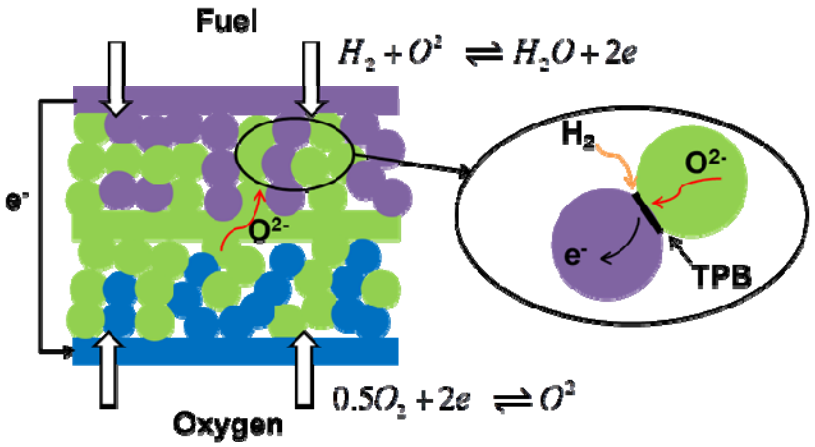
Fuel
$H_2 + O^2 \rightleftharpoons H_2O + 2e$
e-
O2-
H2
O2-
e-
TPB
Oxygen
$0.5O_2 + 2e \rightleftharpoons O^2$

Fig. 1

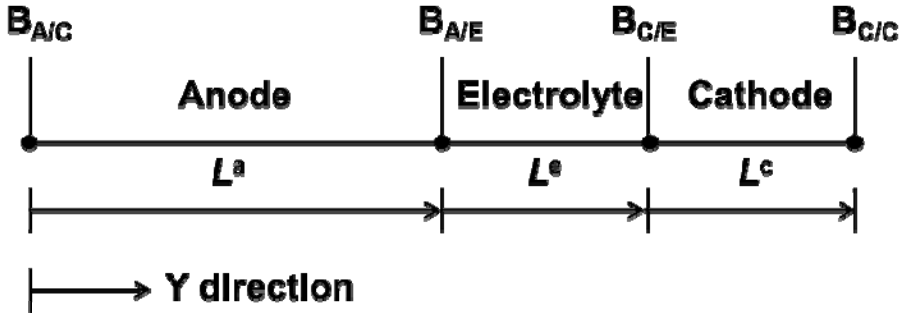
$B_{A/C}$
$B_{A/E}$
$B_{C/E}$
$B_{C/C}$
Anode
Electrolyte
Cathode
L^a
L^e
L^c
Y direction

Fig. 2

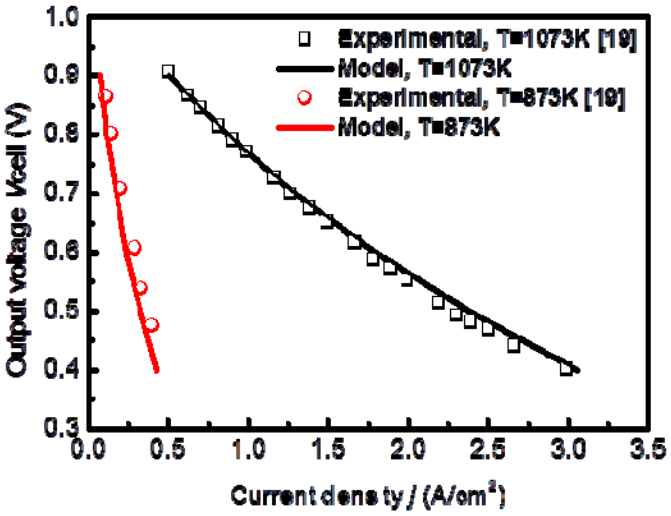
Experimental, T=1073K [19]
Model, T=1073K
Experimental, T=873K [19]
Model, T=873K
Output voltage Vcell (V)
Current density j (A/cm²)
1.0
0.9
0.8
0.7
0.6
0.5
0.4
0.3
0.0
0.5
1.0
1.5
2.0
2.5
3.0
3.5

Fig. 3

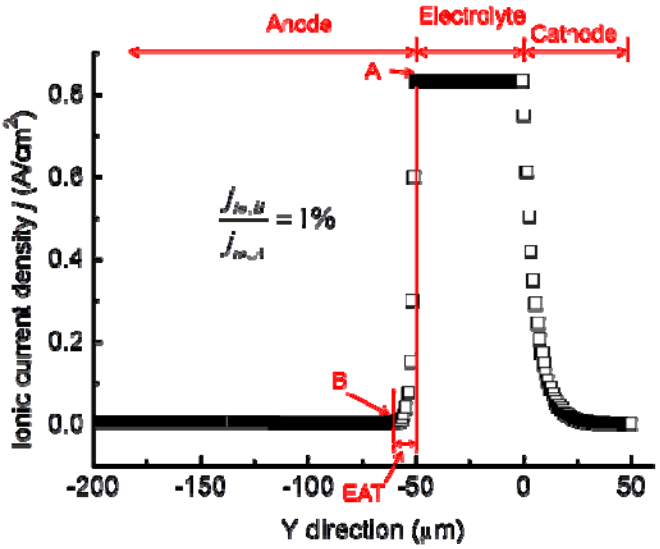
Anode
Electrolyte
Cathode
A
B
EAT
0.8
0.6
0.4
0.2
0.0
-200
-150
-100
-50
0
50
Ionic current density j (A/cm²)
Y direction (μm)

Fig. 4

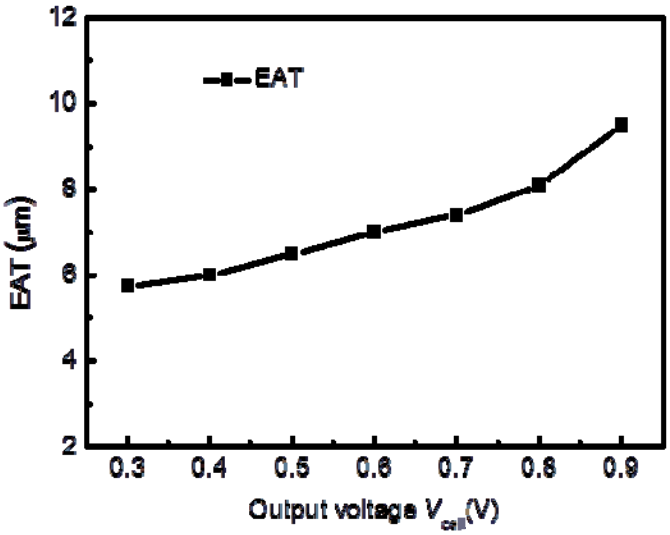

Fig. 5

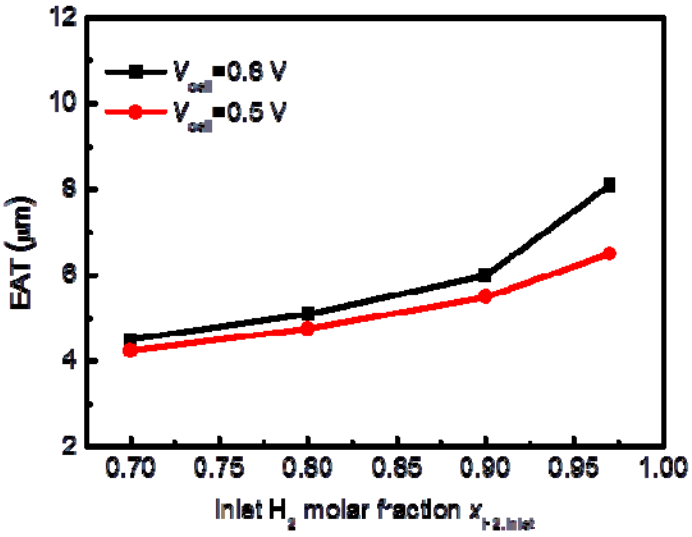
12
10
8
6
4
2
EAT (μm)
V_{cell}=0.6 V
V_{cell}=0.5 V
0.70
0.75
0.80
0.85
0.90
0.95
1.00
Inlet H_2 molar fraction $x_{H2,Inlet}$

Fig. 6

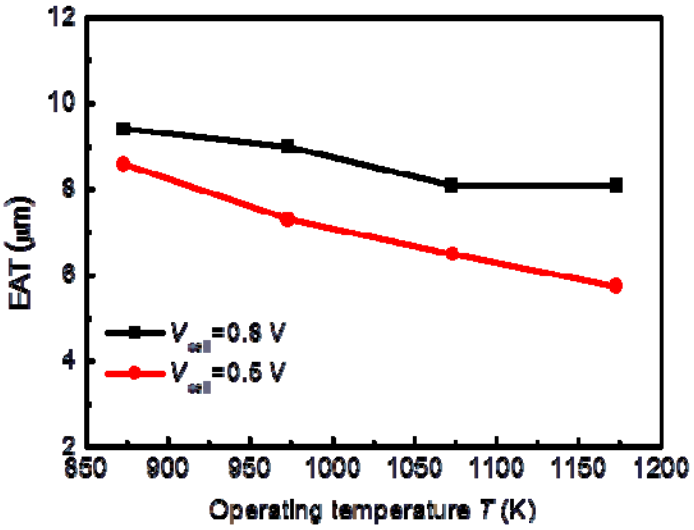
12
10
8
6
4
2
EAT (μm)
V_{cell}=0.8 V
V_{cell}=0.5 V
850
900
950
1000
1050
1100
1150
1200
Operating temperature T (K)

Fig. 7

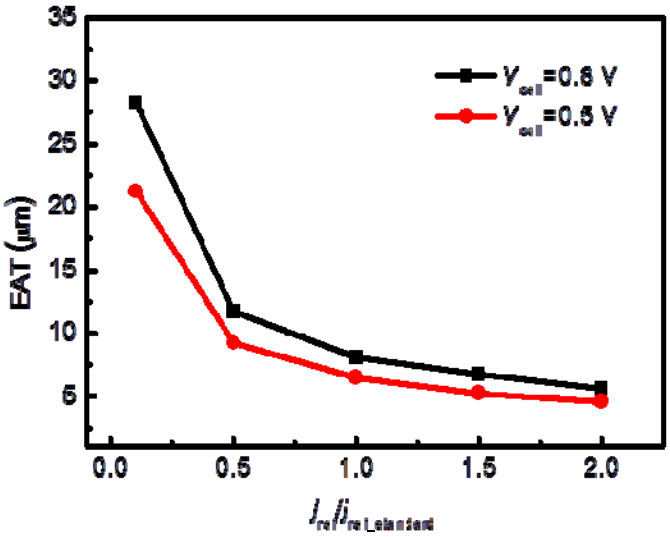

Fig. 8

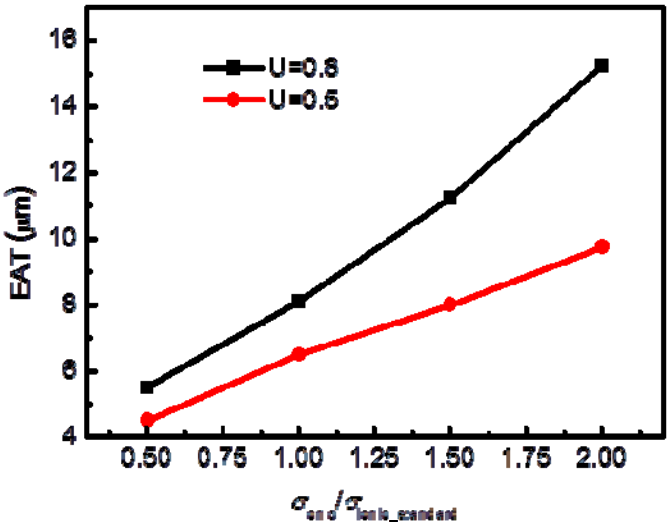
U=0.8
U=0.5
EAT (μm)
16
14
12
10
8
6
4
0.50
0.75
1.00
1.25
1.50
1.75
2.00
$\sigma_{cnd}/\sigma_{lamb\_constant}$

Fig. 9

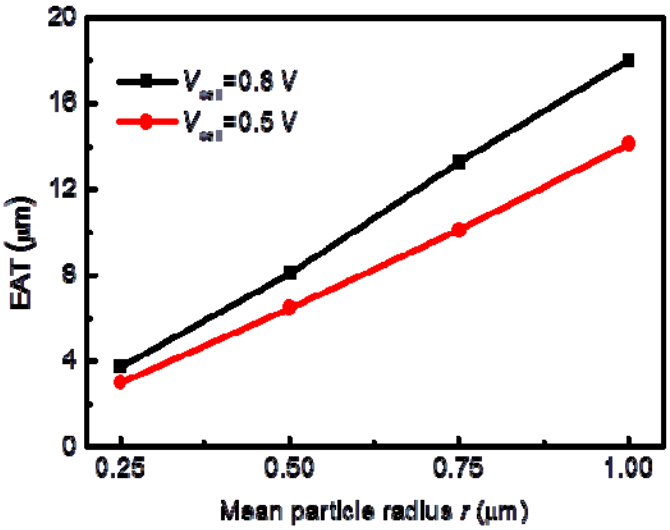
20
16
12
8
4
0
EAT (μm)
V_{cell}=0.8 V
V_{cell}=0.5 V
0.25
0.50
0.75
1.00
Mean particle radius r (μm)

Fig. 10

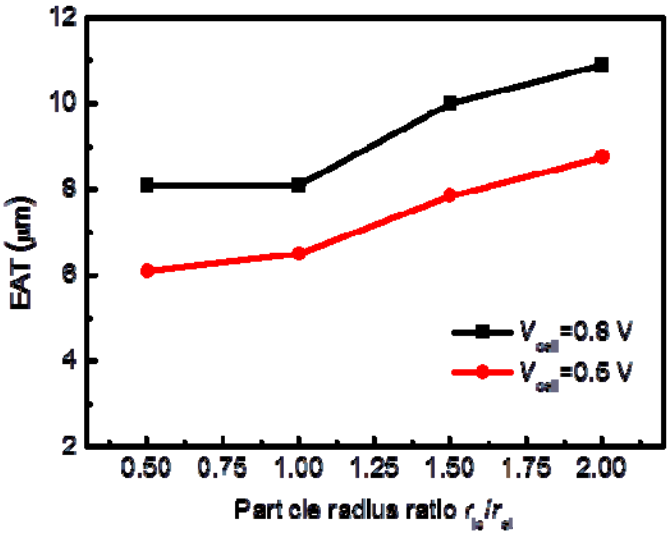
12
10
8
6
4
2
EAT (μm)
0.50
0.75
1.00
1.25
1.50
1.75
2.00
Particle radius ratio r_{ip}/r_{el}
V_{cell}=0.8 V
V_{cell}=0.5 V

Fig. 11

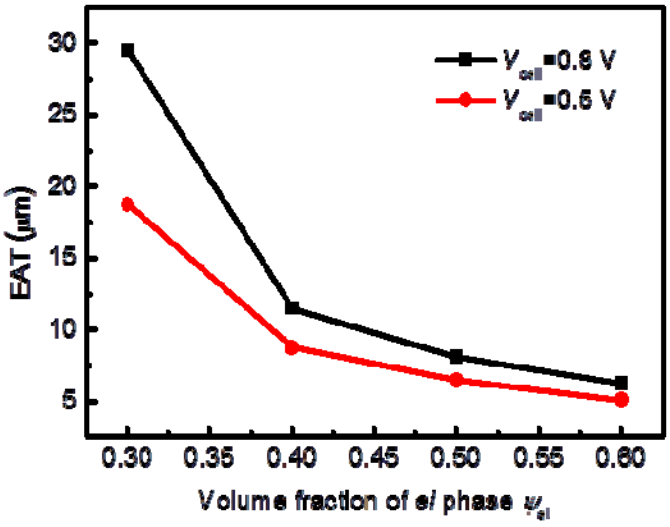
30
25
20
15
10
5
EAT (μm)
0.30
0.35
0.40
0.45
0.50
0.55
0.60
Volume fraction of ei phase ψei
Vcell=0.8 V
Vcell=0.6 V

Fig. 12

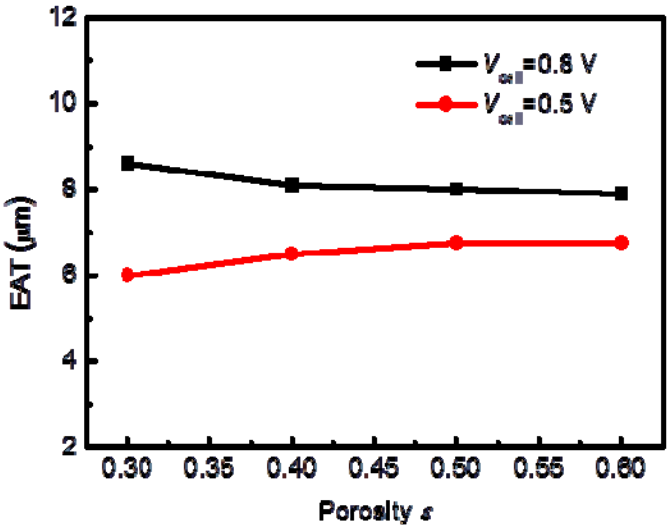
12
10
8
6
4
2
EAT (μm)
0.30
0.35
0.40
0.45
0.50
0.55
0.60
Porosity ε
V_{coil}=0.6 V
V_{coil}=0.5 V

Fig. 13

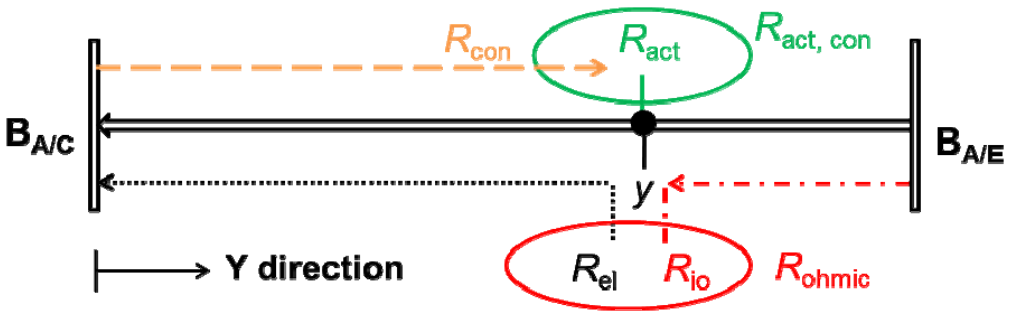

Fig. 14